Magnetic phase transitions in the anion-deficient $La_{1-x}Ba_xMnO_{3-x/2}$ ($0 \leq x \leq 0.50$) manganites

2003 J. Phys.: Condens. Matter 15 1783

(http://iopscience.iop.org/0953-8984/15/10/324)

INSTITUTE OF PHYSICS PUBLISHING JOURNAL OF PHYSICS: CONDENSED MATTER

J. Phys.: Condens. Matter **15** (2003) 1783–1795 PII: S0953-8984(03)56529-8

Magnetic phase transitions in the anion-deficient $La_{1-x}Ba_xMnO_{3-x/2}$ ($0 \leqslant x \leqslant 0.50$) manganites

S V Trukhanov[1,3], L S Lobanovski[1], M V Bushinsky[1], I O Troyanchuk[1] and H Szymczak[2]

[1] Institute of Solids and Semiconductor Physics, NAS, P Brovka Street 17, 220072 Minsk, Belarus
[2] Institute of Physics, PAS, Lotnikov Street 32/46, 02-668 Warsaw, Poland

E-mail: truhanov@ifttp.bas-net.by

Received 22 November 2002, in final form 16 January 2003
Published 3 March 2003
Online at stacks.iop.org/JPhysCM/15/1783

Abstract

The crystal structure, magnetization and electrical resistivity properties of the anion-deficient $La_{1-x}Ba_xMnO_{3-x/2}$ ($0 \leqslant x \leqslant 0.50$) perovskite manganites without Mn^{4+} ions have been investigated. It is established the reduced samples in the region $0 \leqslant x \leqslant 0.05$ are O′-orthorhombic perovskites, in $0.10 \leqslant x \leqslant 0.25$ they are rhombohedric whereas in $0.27 \leqslant x \leqslant 0.50$ they are cubic. It is found that, as the x doping level increases, the samples undergo a transition from a weak ferromagnetic state ($x = 0$) to an inhomogeneous ferromagnetic one, ($x \geqslant 0.03$) being a mixture of antiferromagnetic and ferromagnetic phases. At $x \geqslant 0.12$ competition between antiferromagnetic and ferromagnetic interactions leads to a cluster spin glass state appearance with a magnetic moment freezing temperature of ∼45 K. The dominant magnetic phase for $x \geqslant 0.22$ is supposed to be antiferromagnetic. All the reduced samples are semiconductors and show considerable magnetoresistance over a wide temperature range in a magnetically ordered state. The largest magnetoresistance (∼34% in a 9 kOe field at liquid nitrogen temperatures) is observed for an $x = 0.30$ sample. The magnetic phase diagram of $La^{3+}_{1-x}Ba^{2+}_xMn^{3+}O^{2-}_{3-x/2}$ manganites has been established by combining the results of magnetic and electrical measurements. The results obtained could be understood in terms of the phase separation and the 180° superexchange Mn^{3+}–O–Mn^{3+} interaction model.

1. Introduction

The hole-doped perovskite manganites with common chemical formula $Ln_{1-x}A_xMnO_3$ (Ln = La, Pr, Nd, etc, A = Ca, Sr, Ba, etc) are prospective magnetic materials. These compounds have a strong correlation between magnetic and electrical properties [1–4].

[3] Author to whom any correspondence should be addressed.

0953-8984/03/101783+13$30.00

The hole-doped $Ln^{3+}_{1-x}A^{2+}_{x}Mn^{3+}_{1-x}Mn^{4+}_{x}O^{2-}_{3}$ manganites in the concentration range $0.20 < x < 0.50$ usually exhibit a metal–insulator (MI) transition at a certain temperature T_{MI} near the Curie point and a sharp magnetoresistance peak slightly below T_{MI} [5, 6]. It is experimentally established that the anomalous transport phenomena in these systems are closely related to their magnetic properties such as the ferromagnetic–paramagnetic phase transition upon heating [7]. The discovery of the CMR phenomenon in the hole-doped manganites made possible the application of these compounds to magnetic recording techniques [8–10].

A Zener double-exchange (DE) interaction has been proposed as the cause of the metallic behaviour and of the strong ferromagnetic interactions between Mn ions. This model is based on the real exchange of electrons between Mn^{3+} and Mn^{4+} ions [11, 12]. The existence of Mn^{4+} ions is conditioned with the substitution of Ln^{3+} ions by divalent alkaline-earth A^{2+} ions [13].

One should note that a deviation from oxygen stoichiometry also leads to a mixed valence of Mn ions. The introduction of one oxygen vacancy in compounds transforms two neighbouring Mn^{3+} ions to Mn^{4+} ones. At $\gamma = x/2$ the given compositions contain only Mn^{3+} ions [14]. It is attractive that the perovskite manganites have an extensive oxygen nonstoichiometry, in contrast with the other transition metal oxides with perovskite structures. The oxygen content in the manganites may vary from 2.5 [15] to 3.27 [16]. A much smaller degree of oxygen nonstoichiometry has been found for $LaVO_{3+\gamma}$ ($0 \leqslant \gamma \leqslant 0.05$) and $LaTiO_{3+\gamma}$ ($0 \leqslant \gamma \leqslant 0.08$) while $LaCr_3$ and $LaFeO_3$ do not reveal quite such a deviation from stoichiometry [17].

It is worth noting that Ba-doped manganites are much less studied than others. As was known an upper limit of barium substitution for those samples prepared in air is slightly below $x = 0.50$ [18]. It is due to the eventual formation of a hexagonal $BaMnO_3$-type perovskite at the grain boundaries [19]. However, recently the homogeneity range of these oxides was found to extend up to $x = 2/3$ due to a realization of two-step reduction–reoxidation synthesis [20].

Among other manganites the Ba-substituted ones offer particular interest because they exhibit long-range ferromagnetic order and large magnetoresistance above room temperature. For example, $La_{0.65}Ba_{0.35}MnO_3$ has $T_C = 362$ K. Such a high T_C value results from the relatively large average size of the A-site cation in the case of Ba doping, since it has been shown that T_C increases as $\langle r_A \rangle$ increases [21].

In this paper we present the magnetic and electrical properties of reduced $La^{3+}_{1-x}Ba^{2+}_{x}Mn^{3+}O^{2-}_{3-x/2}$ ($0 \leqslant x \leqslant 0.50$) manganites without Mn^{4+} ions.

2. Experiment

The polycrystalline $La_{1-x}Ba_xMnO_3$ ($x = 0$, 0.03, 0.05, 0.10, 0.12, 0.15, 0.17, 0.20, 0.22, 0.25, 0.27, 0.30, 0.32, 0.35, 0.37, 0.40, 0.42, 0.45, 0.47, 0.50) samples have been obtained from high purity (>99.999%)La_2O_3, Mn_2O_3 and $BaCO_3$ using the standard ceramic method. The powders have been mixed in the desired ratio (La:Ba:Mn $= [1 - x]$:x:1) and pressed into 20 mm pellets. Before weighing, La_2O_3 has been annealed in air at 1000 °C for 2 h to remove H_2O and CO_2. Prefiring of the samples has been performed at 1000 °C in air over 5 h to ensure complete decomposition of carbonates. After igniting the pellets have again been ground and pressed. Final synthesis has been realized in air at 1550 °C for 10 h followed by quenching of the samples with a low ($x < 0.20$) concentration of Ba ions from 1000 °C and slow cooling of the samples with a high ($x > 0.30$) concentration of Ba ions in the furnace at a rate of 80 °C h^{-1} in order to achieve stoichiometric oxygen content. During the prefiring and final synthesis the samples have been situated on a platinum substrate. The purity of the samples has been checked by x-ray powder diffraction (XRD) with a DRON-3 diffractometer

in Cr Kα radiation at room temperature. The XRD patterns have been collected over an angle range of $30° \leqslant 2\Theta \leqslant 100°$. An initial oxygen content of the as-prepared samples has been determined by thermogravimetric analysis (TGA). These investigations have shown the oxygen concentration to be slightly above the stoichiometric value for all the samples in the $0 \leqslant x \leqslant 0.17$ range. The oxygen excess decreases linearly from $\delta \sim 0.11$ ($x = 0$) down to $\delta \sim 0$ ($x = 0.20$). At $0.20 \leqslant x \leqslant 0.37$ the oxygen content corresponds to stoichiometry $\delta \sim 0$ and at $0.40 \leqslant x \leqslant 0.50$ it is slightly below (oxygen deficit $\gamma \sim 0.02$; $\gamma = -\delta$).

In order to prepare stoichiometric samples the compositions in the range $0 \leqslant x \leqslant 0.17$ have been annealed in evacuated silica ampoules at 700 °C for 30 h in the presence of metallic Ta as an oxygen getter. The amount of Ta has been calculated supposing the final products to be Ta_2O_5 and stoichiometric compositions $La_{1-x}Ba_xMnO_3$ according to the relation (1)

$$La_{1-x}Ba_xMnO_{3+\gamma} + (2\gamma/5) \cdot Ta \longrightarrow La_{1-x}Ba_xMnO_3 + (\gamma/5) \cdot Ta_2O_5. \quad (1)$$

In contrast, the samples with $0.40 \leqslant x \leqslant 0.50$ have been annealed in air at 1000 °C for 80 h. These reactions can be described by

$$La_{1-x}Ba_xMnO_{3-\gamma} + (\gamma/2) \cdot O_2 \longrightarrow La_{1-x}Ba_xMnO_3. \quad (2)$$

The weight loss and gain of the samples before and after the applied annealing procedures have been used to check the oxygen stoichiometry. These investigations, as well as TGA measurements, have shown the oxygen content of such prepared samples to be stoichiometric.

The oxygen-deficient $La_{1-x}Ba_xMnO_{3-x/2}$ ($x = 0, 0.03, 0.05, 0.10, 0.12, 0.15, 0.17, 0.20, 0.22, 0.25, 0.27, 0.30, 0.32, 0.35, 0.37, 0.40, 0.42, 0.45, 0.47, 0.50$) samples have been produced by the topotactic reduction procedure. These reactions have been realized in accordance with equation (3):

$$La_{1-x}Ba_xMnO_3 + (x/5) \cdot Ta \longrightarrow La_{1-x}Ba_xMnO_{3-x/2} + (x/10) \cdot Ta_2O_5. \quad (3)$$

The oxygen deficit in reduced samples has been calculated from a change of weight of the samples after reduction. A sample of 2–3 g has usually been placed into a silica ampoule. The relative error in the oxygen content measurements did not exceed 0.3%. Therefore, the chemical formula of the reduced samples may be written as $La_{1-x}Ba_xMnO_{3-x/2\pm0.01}$.

The temperature and field dependencies of the magnetization have been registered with an OI-3001 vibrating sample magnetometer in a temperature range of 4–300 K. Zero field cooled (ZFC) and field cooled (FC) magnetization measurements have been realized. In order to determine the magnetic ordering temperature T_{MO} the samples have been slowly warmed in a low external magnetic field (100 Oe). T_{MO} has been taken as the minimum of the FC magnetization derivative, depending on the temperature. We have also used one more critical temperature T_{CR} at which ZFC magnetization reaches its maximal value. The spontaneous magnetization value M_S has been determined from the field dependence of the magnetization at 6 K by extrapolation of the linear part of the curve to zero field. These measurements have been taken in a field-decreasing regime. The dc resistivity data have been collected by a four-probe method on well-sintered samples in the form of bars with dimensions $10 \times 2 \times 2$ mm^3 over a temperature range 77–300 K. Indium eutectic has been employed for ultrasonic forming of the contacts. The magnetoresistance has been calculated according to the relation (4)

$$MR(\%) = [\rho(H) - \rho(H = 0)]/\rho(H = 0) \cdot 100\% \quad (4)$$

where MR is the magnetoresistance, $\rho(H)$ is the resistivity in a magnetic field of 9 kOe and $\rho(H = 0)$ is the resistivity without a magnetic field. The magnetic field has been applied in parallel to the electric current in the sample.

Table 1. Symmetry and parameters (a, b, c, α and V) of the unit cell for the stoichiometric $La_{1-x}Ba_xMnO_3$ samples. O′ denote O′ orthorhombic symmetry, R rhombohedric and C cubic.

Composition	Symmetry	a (Å)	b (Å)	c (Å)	α (Å)	V (Å^3)
$LaMnO_3$	O′	5.537	5.749	7.692		244.72
$La_{0.97}Ba_{0.03}MnO_3$	O′	5.526	5.684	7.778		244.31
$La_{0.95}Ba_{0.05}MnO_3$	O′	5.519	5.672	7.796		244.04
$La_{0.90}Ba_{0.10}MnO_3$	R	3.933			90.65	60.85
$La_{0.88}Ba_{0.12}MnO_3$	R	3.931			90.56	60.76
$La_{0.85}Ba_{0.15}MnO_3$	R	3.929			90.44	60.67
$La_{0.83}Ba_{0.17}MnO_3$	R	3.928			90.31	60.60
$La_{0.80}Ba_{0.20}MnO_3$	R	3.926			90.23	60.50
$La_{0.78}Ba_{0.22}MnO_3$	R	3.924			90.15	60.44
$La_{0.75}Ba_{0.25}MnO_3$	R	3.925			90.05	60.34
$La_{0.73}Ba_{0.27}MnO_3$	C	3.921				60.27
$La_{0.70}Ba_{0.30}MnO_3$	C	3.919				60.18
$La_{0.68}Ba_{0.32}MnO_3$	C	3.917				60.11
$La_{0.65}Ba_{0.35}MnO_3$	C	3.915				59.99
$La_{0.63}Ba_{0.37}MnO_3$	C	3.913				59.93
$La_{0.60}Ba_{0.40}MnO_3$	C	3.911				59.84
$La_{0.58}Ba_{0.42}MnO_3$	C	3.909				59.75
$La_{0.55}Ba_{0.45}MnO_3$	C	3.907				59.65
$La_{0.53}Ba_{0.47}MnO_3$	C	3.906				59.58
$La_{0.50}Ba_{0.50}MnO_3$	C	3.904				59.49

3. Results and discussion

At first let us consider the XRD data. X-ray patterns of the reduced $La^{3+}_{1-x}Ba^{2+}_xMn^{3+}O^{2-}_{3-x/2}$ ($x = 0.03, 0.15, 0.30, 0.45$) samples are presented in figure 1. According to x-ray measurements all the samples have been single-phase perovskites with O′-orthorhombic ($0 \leqslant x \leqslant 0.05$)O′, rhombohedral ($0.10 \leqslant x \leqslant 0.25$)R and cubic ($0.27 \leqslant x \leqslant 0.50$)C unit cells. The reduction procedure has not changed the lattice symmetry. Crystal structure parameters for both stoichiometric and reduced series are given in tables 1 and 2. According to Goodenough [22], O′-distortion ($c/\sqrt{2} < a \leqslant b$) is caused by an orbital ordering, which is a result of the cooperative static Jahn–Teller effect. This takes place in $LaMnO_3$, being a Jahn–Teller system with Mn^{3+} ions only. As the dopant ion concentration increases above a critical value ($x \sim 0.10$) the cooperative static Jahn–Teller distortion becomes local and dynamic [23]. In this case the transition from O′-orthorhombic distortion to O-orthorhombic ($a < c/\sqrt{2} < b$) usually occurs. Nevertheless, we have observed a O′ → R transition at $x \sim 0.10$. It is possible that a size effect for Ba-doped manganites dominates over the Jahn–Teller one and the R phase is formed. All the reduced samples have only Mn^{3+} ions. However, the $\gamma = 0.025$ oxygen vacancy concentration is not large enough to remove the orbital ordering and produce the O phase. At $x \geqslant 0.10$ the orbital ordering is removed.

For both the stoichiometric and reduced series of samples the comparative volume of the unit cell decreases gradually as barium content increases (figure 2). However, this process is much less pronounced for the reduced series. The substitution of La^{3+} by Ba^{2+} for stoichiometric samples produces Mn^{4+} ions. La^{3+} and Ba^{2+} ions in 12-fold coordination have effective ionic radii of 1.36 and 1.61 Å, respectively [24]. It is well known that the Mn^{3+} ionic radius is larger than that of Mn^{4+}. The effective ionic radii of Mn^{3+} and Mn^{4+} in octahedral oxygen coordination are 0.645 and 0.530 Å, respectively [24]. So the size effect of the $Mn^{3+} \rightarrow Mn^{4+}$ process appears to dominate over the $La^{3+} \rightarrow Ba^{2+}$ one, which leads to a

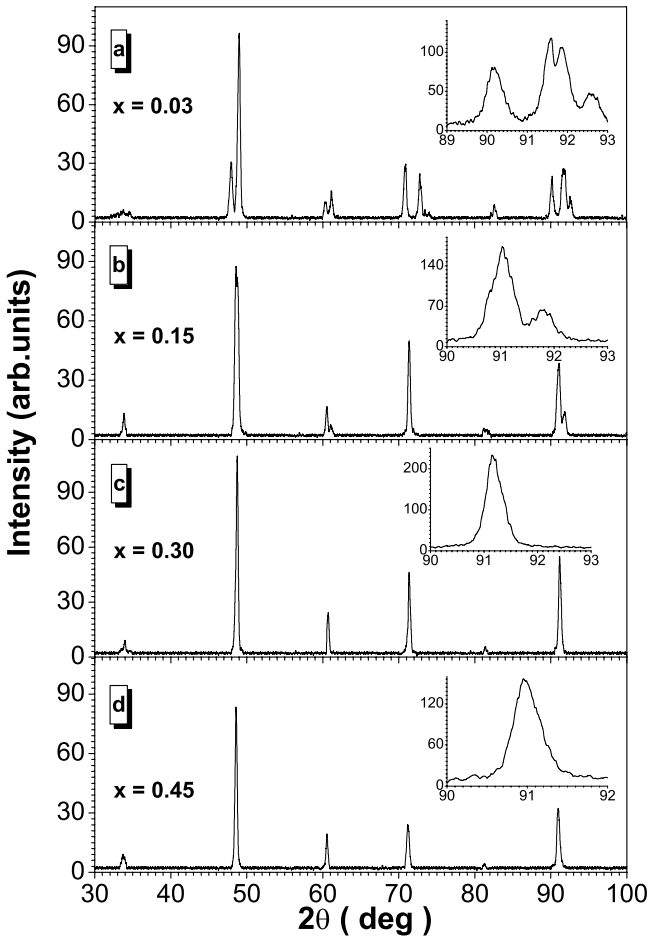

Figure 1. Powder x-ray diffraction patterns at room temperature for the reduced $La_{1-x}Ba_xMnO_{3-x/2}$ samples with $x = 0.03$ (a), 0.15 (b), 0.30 (c), 0.45 (d). Insets demonstrate $132 + 024 + 312 + 204$ (a), $21\bar{1} + 211 + \bar{2}11$ (b), 211 (c) and 211 (d) reflexes.

decrease in unit cell volume as doping level increases. The appearance of oxygen vacancies leads to a decreasing average oxidation state of manganese and its coordination. The vacancies should reduce the unit cell volume whereas the $Mn^{4+} \rightarrow Mn^{3+}$ process must increase it. Our data indicate that the first process is more significant.

To determine the magnetic ordering temperature of the reduced $La^{3+}_{1-x}Ba^{2+}_{x}Mn^{3+}O^{2-}_{3-x/2}$ samples ZFC and FC magnetization measurements have been carried out in a field of 100 Oe (figures 3 and 4).

The samples with $x = 0.03$ and 0.05 (figure 3) demonstrate an increase of FC magnetization below 144 and 150 K, respectively. It is worth nothing that these temperatures are close to $T_N \approx 143$ K for $LaMnO_3$ [13]. The ZFC curve starts to differ significantly from the FC one just below T_{MO}, at which point it has a small peak and does not depend on temperature in practice. It may be in the case of a large magnetic anisotropy.

At $0.10 \leqslant x \leqslant 0.20$ ZFC and FC curves differ well below the T_{MO} and the difference between them gradually increases as temperature decreases. The transition to a paramagnetic

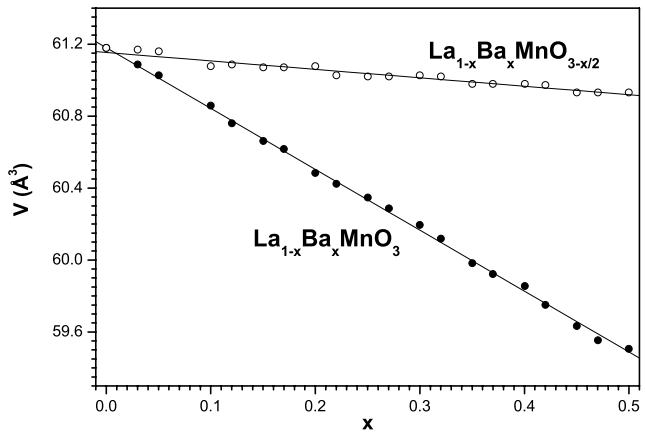

Figure 2. Comparative volume of unit cell versus doping level for both the stoichiometric (full circles) and reduced (open circles) $La_{1-x}Ba_xMnO_{3-x/2}$ ($0 \leqslant x \leqslant 0.50$) samples. The straight lines are guides for the eyes.

Table 2. Symmetry and parameters (a, b, c, α and V) of the unit cell for the reduced $La_{1-x}Ba_xMnO_{3-x/2}$ samples. O′ denote O′ orthorhombic symmetry, R rhombohedric and C cubic.

Composition	Symmetry	a (Å)	b (Å)	c (Å)	α (Å)	V (Å^3)
$LaMnO_3$	O′	5.537	5.749	7.692		244.72
$La_{0.97}Ba_{0.03}MnO_{2.99}$	O′	5.529	5.688	7.780		244.67
$La_{0.95}Ba_{0.05}MnO_{2.98}$	O′	5.524	5.675	7.802		244.58
$La_{0.90}Ba_{0.10}MnO_{2.95}$	R	3.939			90.41	61.13
$La_{0.88}Ba_{0.12}MnO_{2.94}$	R	3.939			90.35	61.12
$La_{0.85}Ba_{0.15}MnO_{2.93}$	R	3.938			90.29	61.09
$La_{0.83}Ba_{0.17}MnO_{2.92}$	R	3.938			90.23	61.08
$La_{0.80}Ba_{0.20}MnO_{2.90}$	R	3.938			90.16	61.07
$La_{0.78}Ba_{0.22}MnO_{2.89}$	R	3.937			90.09	61.04
$La_{0.75}Ba_{0.25}MnO_{2.88}$	R	3.937			90.02	61.03
$La_{0.73}Ba_{0.27}MnO_{2.87}$	C	3.937				61.02
$La_{0.70}Ba_{0.30}MnO_{2.85}$	C	3.937				61.02
$La_{0.68}Ba_{0.32}MnO_{2.84}$	C	3.937				61.02
$La_{0.65}Ba_{0.35}MnO_{2.83}$	C	3.936				60.98
$La_{0.63}Ba_{0.37}MnO_{2.82}$	C	3.936				60.98
$La_{0.60}Ba_{0.40}MnO_{2.80}$	C	3.936				60.98
$La_{0.58}Ba_{0.42}MnO_{2.79}$	C	3.936				60.98
$La_{0.55}Ba_{0.45}MnO_{2.78}$	C	3.935				60.93
$La_{0.53}Ba_{0.47}MnO_{2.77}$	C	3.935				60.93
$La_{0.50}Ba_{0.50}MnO_{2.75}$	C	3.935				60.93

state is well defined, which is characteristic of homogeneous magnetic materials. The sample with $x = 0.15$ demonstrates the weakest $T_{MO} = 124$ K. T_{CR} smoothly decreases from 132 K ($x = 0.10$) to 94 K ($x = 0.15$).

In the region $0.22 \leqslant x \leqslant 0.32$ the ZFC magnetization (figure 4) shows a pronounced peak at ∼45 K. Below this peak ZFC decreases with temperature. This is attributed to a spin freezing behaviour. So the temperature of this peak has been taken as a spin cluster freezing one T_{FR}. In this region T_{FR} coincides with T_{CR}. The transition to a demagnetized state is

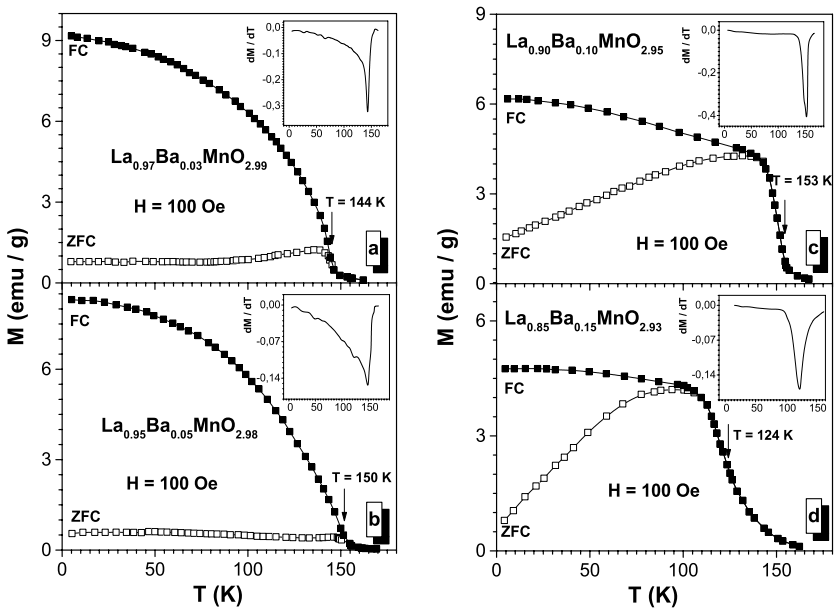

Figure 3. ZFC (open symbols) and FC (full symbols) magnetizations versus temperature in a magnetic field of 100 Oe for the reduced $La_{1-x}Ba_xMnO_{3-x/2}$ samples with $x = 0.03$ (a), 0.05 (b), 0.10 (c), 0.15 (d). Insets demonstrate the temperature dependence of the FC magnetization derivative.

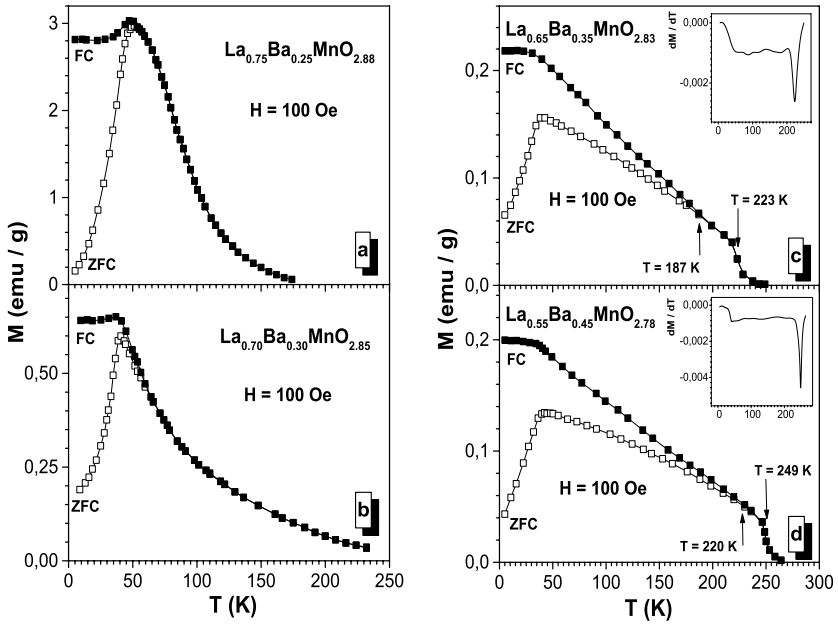

Figure 4. ZFC (open symbols) and FC (full symbols) magnetizations versus temperature in a magnetic field of 100 Oe for the reduced $La_{1-x}Ba_xMnO_{3-x/2}$ samples with $x = 0.25$ (a), 0.30 (b), 0.35 (c), 0.45 (d). Insets demonstrate the temperature dependence of the FC magnetization derivative.

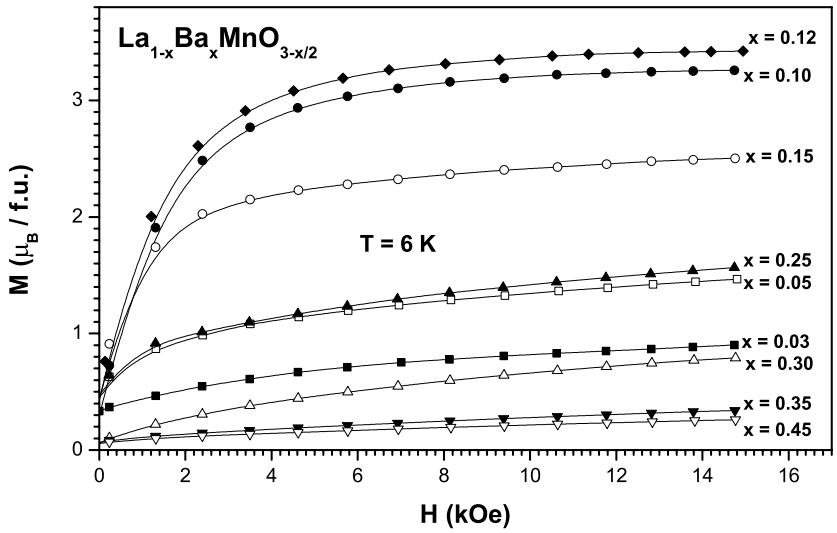

Figure 5. Magnetization versus field at $T = 6$ K for the reduced $La_{1-x}Ba_xMnO_{3-x/2}$ samples with $x = 0.03$ (full rectangles), 0.05 (open rectangles), 0.10 (full circles), 0.15 (open circles), 0.25 (full up-triangles), 0.30 (open up-triangles), 0.35 (full down-triangles) and 0.45 (open down-triangles).

broad enough and we did not use the standard procedure to definite T_{MO} for these samples. This broad transition may also be characteristic of an inhomogeneous initial magnetic state.

At $0.35 \leqslant x \leqslant 0.50$ samples demonstrate almost linear FC magnetization dependencies with a sharp drop at about 220–250 K. T_{FR} is almost constant in this region. It is notable that the ZFC and FC magnetization divergence temperature T_{DV} continuously increases from 187 K ($x = 0.35$) up to 220 K ($x = 0.45$).

In figure 5 the magnetization is shown as a function of magnetic field at a temperature of 6 K for some reduced $La^{3+}_{1-x}Ba^{2+}_{x}Mn^{3+}O^{2-}_{3-x/2}$ ($x = 0.03$, 0.05, 0.10, 0.12, 0.15, 0.25, 0.30, 0.35, 0.45) samples. It is difficult to estimate M_S unambiguously because the magnetization for a majority of the reduced samples is not saturated in a field up to 16 kOe. As is shown from figure 5 M_S first increases almost linearly as the Ba content increases, reaching the maximum value of 3.14 μ_B/f.u. at $x = 0.12$, and then steadily decreases down to 0.04 μ_B/f.u. ($x = 0.50$). Even in the case of $x = 0.12$ there is no pure ferromagnetic ordering because an expected value is around 4 μ_B/f.u. for a parallel arrangement of all the Mn^{3+} magnetic moments. It is worth noting that the samples with $x = 0.03$ and 0.05 have a coercive field large enough.

Electrical resistivity and magnetoresistance versus temperature for the reduced $La^{3+}_{1-x}Ba^{2+}_{x}Mn^{3+}O^{2-}_{3-x/2}$ ($x = 0.05$, 0.15, 0.30, 0.45) samples are displayed in figure 6. All the reduced samples have a resistivity of the activation type. There is no MI transition even for the $x = 0.12$ sample showing the largest ferromagnetic component. The resistivity always increases as temperature decreases. At room temperature resistivity of the reduced samples gradually decreases as doping level increases and at $x = 0.30$ it starts to rise up to $x = 0.50$. All the reduced samples show a magnetoresistance below a point where spontaneous magnetization develops. There is no peak of magnetoresistance as in the case of classic magnetic semiconductors. The gradual magnetoresistance increase up to liquid nitrogen temperature has been observed, which is typical for conducting magnetic ceramics. The maximum MR = 34% has been observed for $x = 0.30$. This type of magnetoresistance is possible due to an intergranular electrical transport.

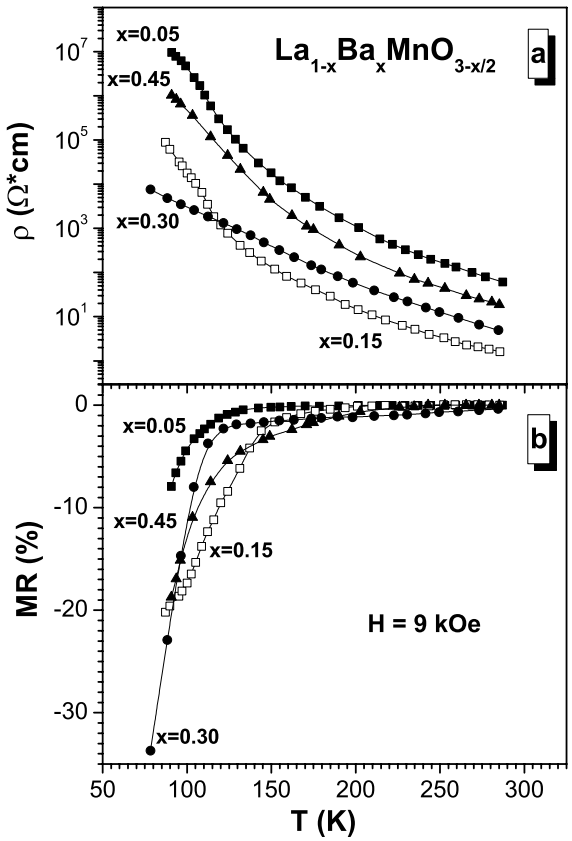

Figure 6. Resistivity (a) and magnetoresistance (b) in a magnetic field of 9 kOe versus temperature for the reduced $La_{1-x}Ba_xMnO_{3-x/2}$ samples with $x = 0.05$ (full rectangles), 0.15 (open rectangles), 0.30 (full circles) and 0.45 (full up-triangles).

Figure 7 demonstrates the dependencies of spontaneous magnetization and magnetic phase diagram for the reduced samples. Increasing Ba content up to $x = 0.12$ leads to an increase (approximately linear) of the spontaneous magnetization from $M_S \sim 0.1$ ($x = 0$) to $\sim$3.14 μ_B/f.u. ($\sim$80% of the expected value for the truly ferromagnetic ordering of $x = 0.12$) and then it drops down to 0.04 μ_B/f.u. ($x = 0.50$). The decrease in M_S occurs through two line sections with a crossing point at $x = 0.27$.

Summarizing our magnetization and electrical data, we construct the hypothetical magnetic phase diagram of the reduced $La^{3+}_{1-x}Ba^{2+}_xMn^{3+}O^{2-}_{3-x/2}$ ($0 \leqslant x \leqslant 0.50$) series. The phase diagram of the stoichiometric $La^{3+}_{1-x}Ba^{2+}_xMn^{3+}_{1-x}Mn^{4+}_xO^{2-}_3$ ($0 \leqslant x \leqslant 0.50$) compounds may be obtained elsewhere [25–29]. Five principal regions are delineated in figure 7. As is noted above $LaMnO_3$ is an A-type antiferromagnetic insulator with a small ferromagnetic component due to noncollinearity of the manganese magnetic moments, i.e. weak ferromagnet. An orbital ordering is observed in $LaMnO_3$ and the superexchange magnetic interactions of manganese ions are anisotropic (positive in the (001) plane and negative along the [001] direction) as a result of the Jahn–Teller effect. The ferromagnetic component starts to increase for $x = 0.03$ and 0.05. However, we believe that the ground state in this range is antiferromagnetic, similar to $LaMnO_3$.

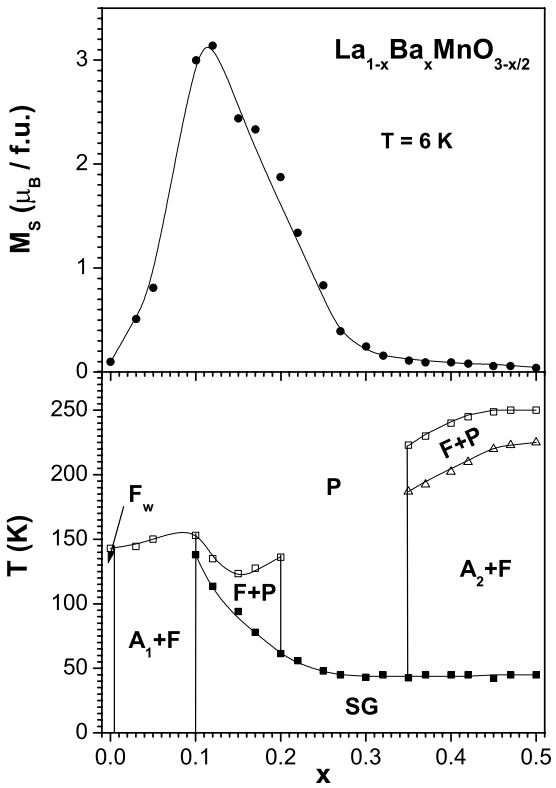

Figure 7. Dependencies of spontaneous magnetization (full circles) (a) and magnetic ordering temperature (rectangles and up-triangles) with assumed magnetic states (b). F_w denotes a weak ferromagnet, A_1 + F a mixture of antiferromagnetic (orbital ordered) and ferromagnetic phases, A_2 + F a mixture of antiferromagnetic (orbital disordered due to an oxygen vacancies appearance) and ferromagnetic phases and F + P an inhomogeneous ferromagnet, where SG is a cluster spin glass state and P a paramagnet.

At $0.10 \leqslant x \leqslant 0.20$ ZFC magnetization displays a spin freezing behaviour, which is characterized by a broad maximum. The absence of a sharp cusp on the ZFC curve and a large spontaneous magnetization indicate that a ferromagnetic order exists above T_{CR}. Traditionally, the reduced M_S has been explained by the spin canting [12, 13]. The reduced M_S may also be explained by a spin cluster model in a phase separation scenario. In that local ferromagnetic regions are placed into either an antiferromagnetic or paramagnetic matrix. Since it is well known that the canted magnetic structure should be the result of the DE between Mn^{3+} and Mn^{4+} ions and the $La^{3+}_{1-x}Ba^{2+}_{x}Mn^{3+}O^{2-}_{3-x/2}$ does not contain Mn^{4+}, we assume that the ferromagnetic component for $0.10 \leqslant x \leqslant 0.20$ results from superexchange interactions between Mn^{3+}–O–Mn^{3+}. As is known [22, 30], the superexchange Mn^{3+}–O–Mn^{3+} magnetic interactions should be positive in the orbitally disordered phase if manganese ions are surrounded by six oxygen anions. However, these interactions became antiferromagnetic in the case of five-fold coordination of the manganese ions [31]. So in this concentration range the oxygen vacancies remove the orbital ordering but they cannot produce the considerable volume of the antiferromagnetic orbital disordered phase.

In the range $0.22 \leqslant x \leqslant 0.32$ the samples have cluster spin glass properties. As the oxygen vacancy number increases the antiferromagnetic (disordered) part of the superexchange

interactions is enhanced. Antiferromagnetic and ferromagnetic phase volumes apparently become comparable. The spin freezing behaviour is often observed in inhomogeneous magnetic systems such as granular films of Co–Cu and Co–Ag [32, 33], where ferromagnetic grains are embedded in a non-ferromagnetic background. For $Eu_xSr_{1-x}S$, the first-neighbour Eu–Eu superexchange interactions are positive, whereas the second-neighbour Eu–Eu ones are negative [34]. The magnetic state of these systems is explained by competition between positive and negative exchange interactions. The competing interactions result in frustration of the clusters which leads to a freezing of the magnetic moment of the clusters along a local easy direction below T_{FR}.

The very small M_S for $0.35 \leqslant x \leqslant 0.50$ suggests the ground state to be antiferromagnetic, ferromagnetic interactions between clusters being reduced. However, antiferromagnetic interactions in this region have different natures than those for the parent $LaMnO_3$. The existence of T_{DV} most likely indicates that the antiferromagnetic interactions have an ordering temperature lower than ferromagnetic ones. Therefore above T_{DV} the samples represent a small volume of the ferromagnetic clusters randomly distributed over the paramagnetic matrix. The large T_{MO} in this region may be explained by ordering oxygen vacancies, which leads to formation of a new phase with particular magnetic and electrical properties. Such a possibility has been examined [35]. At vacancy concentrations exceeding 0.1 at% there will be interactions occurring between the point defects. Depending on the nature of the system these interactions may lead to the formation of extended microdomains which in turn will interact too and form an ordered oxygen-deficient phase.

A simple explanation can be present for the electrical data. Above T_{MO} the samples are paramagnetic insulators and resistivity increases as the temperature decreases. Below T_{MO} different ferromagnetic correlations occur depending on the doping level. However, an appearance of a metallic state is not observed.

As is well known, the parent compound $LaMnO_3$ is a semiconductor. The conductivity mechanism of doped manganites is conditioned by 3d-Mn and 2p-O electronic bands. The replacement of La by Ba ions in $La_{1-x}Ba_xMnO_3$ leads to a decrease in the gap between the 3d-Mn and 2p-O electronic bands. For the stoichiometric compounds above the doping concentration level $x = 0.15$ a pure ferromagnetic state is realized. At concentrations $x > 0.15$ these compounds exhibit MI transition below T_C. This electrotransport behaviour is explained by overlapping of the 3d-Mn and 2p-O bands. The appearance of oxygen vacancies leads to an extending of the crystal lattice and, therefore, to a splitting of the above-mentioned electronic bands. An increase in the concentration of oxygen vacancies (with doping level) leads to an increase in the gap between 3d-Mn and 2p-O bands. It is possible for anion-deficient $La_{1-x}Ba_xMnO_{3-x/2}$ compounds that the doping level $x = 0.15$ is the critical one above which the metallic state and MI transition are not realized, although the ferromagnetic component is significant.

It should also be taken into account that the reduction more likely creates oxygen vacancies at the grain boundaries because diffusion coefficients for oxygen on a grain boundary are larger by one order of magnitude than those in the bulk. The oxygen-poor microdomains appear on the grain surface. As a result the electron transfer between grains is difficult and the resistivity rises. The extraction of oxygen from the grain boundaries leads also to a broadening of the insulating barriers associated with intergrain boundaries so the electrical resistivity should increase too.

Outside the ferromagnetic clusters spin directions are most probably distributed randomly. The carrier transfer from one cluster to another is greatly restricted by randomized spins between clusters. As a result the carriers become immobile and stay inside the clusters. With the increase of the ferromagnetic phase volume for $0 \leqslant x \leqslant 0.15$ the carrier transfer

becomes easier and resistivity decreases. Then resistivity increases for $x > 0.15$ because of the increased spin scattering due to antiferromagnetic interactions. Nevertheless the resistivity of the reduced samples exhibits an insulator behaviour independent of the doping level and temperature. An applied magnetic field suppresses the carrier localization by aligning the magnetic moments, thereby causing a drop in the electrical resistivity, i.e. CMR. The largest MR = 34% observed for the $x = 0.30$ sample is possibly due to the fact that the volumes of the ferromagnetic and antiferromagnetic phases are commensurable and the magnetic field greatly influences the randomized spins.

4. Summary

We have studied the crystal structure, magnetization and electrical resistivity properties of the anion-deficient $La^{3+}_{1-x}Ba^{2+}_{x}Mn^{3+}O^{2-}_{3-x/2}$ ($0 \leqslant x \leqslant 0.50$) perovskite manganites. The reduced samples have been produced by the topotactic reduction procedure. ZFC and FC magnetization measurements have been realized. The M_S has been determined from the field dependence of magnetization. It is found that the samples undergo a transition from a weak ferromagnetic state ($x = 0$) to an inhomogeneous ferromagnetic one ($x \geqslant 0.03$) as doping level increases. At $x \geqslant 0.12$ a competition between antiferromagnetic and ferromagnetic interactions leads to a cluster spin glass state with a magnetic moment freezing temperature of ∼45 K. All the reduced samples are semiconductors and show a considerable magnetoresistance over a wide temperature range in the magnetically ordered state. The magnetic phase diagram of $La^{3+}_{1-x}Ba^{2+}_{x}Mn^{3+}O^{2-}_{3-x/2}$ ($0 \leqslant x \leqslant 0.50$) manganites has been established by combining the results of magnetic and electrical measurements. The obtained results could be understood in terms of the phase separation and the 180° superexchange Mn^{3+}–O–Mn^{3+} interaction model. It is supposed that these interactions became antiferromagnetic in the case of five-fold coordination of the manganese ions. The oxygen vacancies are supposed to be ordered for the strongly reduced ($x \geqslant 0.35$) samples.

Acknowledgments

This work was partly supported by the Fund for Fundamental Research of the Republic of Belarus (project F02M-069) and Polish Committee of Science (KBN grant 5 P03B 016 20).

References

[1] Hawe D 2000 *Sensors Actuators* A **81** 268
[2] von Helmholt R, Wecker J, Holzapfel B, Schultz L and Samwer K 1993 *Phys. Rev. Lett.* **71** 2331
[3] Volger J 1954 *Physica* **20** 46
[4] Kubo K 1972 *J. Phys. Soc. Japan* **33** 21
[5] Chahara K, Ohno T, Kasai M and Kozono Y 1993 *Appl. Phys. Lett.* **63** 1990
[6] Radaelli P G, Cox D E, Marezio M, Cheong S-W, Schiffer P E and Ramirez A P 1995 *Phys. Rev. Lett.* **75** 4488
[7] Lynn J W, Erwin R W, Borchers J A, Huang Q, Santoro A, Peng J-L and Li Z Y 1996 *Phys. Rev. Lett.* **76** 4046
[8] Jin S, McCormack M, Tiefel T H and Ramesh R 1994 *J. Appl. Phys.* **76** 6929
[9] Xu Y, Memmert U and Hartmann U 2001 *Sensors Actuators* A **91** 26
[10] Kostogloudis G Ch and Ftikos Ch 1999 *J. Eur. Ceram. Soc.* **19** 497
[11] Zener C 1951 *Phys. Rev.* **82** 403
[12] de Gennes P G 1960 *Phys. Rev.* **118** 141
[13] Matsumoto G 1970 *J. Phys. Soc. Japan* **29** 606
[14] Briatico J, Alascio B, Allub R, Butera A, Canciro A, Causa M T and Tovar M 1996 *Phys. Rev.* B **53** 14020
[15] Millange F, Caignaert V, Domengés B, Raveau B and Suard E 1998 *Chem. Mater.* **10** 1974
[16] Maurin I, Barboux P, Lassailly Y, Boilot J-P and Villain F 2000 *J. Magn. Magn. Mater.* **211** 139

[17] Tofield B C and Scott W R 1974 *J. Solid State Chem.* **100** 183
[18] Troyanchuk I O, Trukhanov S V, Khalyavin D D and Szymczak H 2000 *J. Magn. Magn. Mater.* **208** 217
[19] Raveau B, Martin C, Maignan A and Hervieu M 2002 *J. Phys.: Condens. Matter* **14** 1297
[20] Yuan S L, Jiang Y, Zeng X Y, Zhao W Y, Yang Y P, Qian J P, Zhang G Q, Tu F and Tang C Q 2000 *Phys. Rev.* B **62** 11347
[21] Millange F, Maignan A, Caignaert V, Simon Ch and Raveau B 1996 *Z. Phys.* B **101** 169
[22] Goodenough J B, Wold A, Arnott R J and Menyuk N 1961 *Phys. Rev.* **124** 373
[23] Troyanchuk I O, Trukhanov S V, Szymczak H, Przewoznik J and Bärner K 2001 *Sov. Phys.–JETP* **93** 161
[24] Shannon R D 1976 *Acta Crystallogr.* A **32** 751
[25] Jonker G H and Van Santen J H 1950 *Physica* **16** 337
[26] Lotgering F K 1970 *Philips Res. Rep.* **25** 8
[27] Roy C and Budhani R C 1999 *J. Appl. Phys.* **85** 3124
[28] Budhani R C, Roy C, Lewis L, Li Q and Moodenbaugh A R 2000 *J. Appl. Phys.* **87** 2490
[29] Ju H L, Nam Y S, Lee J E and Shin H S 2000 *J. Magn. Magn. Mater.* **219** 1
[30] Goodenough J B 1971 *Prog. Solid State Chem.* **5** 149
[31] Poeppelmeier K R, Leonowicz M E and Longo J M 1982 *J. Solid State Chem.* **44** 89
[32] Nafis S, Woollam J A, Shan Z S and Sellmyer D J 1991 *J. Appl. Phys.* **70** 6050
[33] Conde F, Gomez-Polo C and Hernando A 1994 *J. Magn. Magn. Mater.* **138** 123
[34] Moorjani K and Coey J M D 1984 *Magnetic Glasses, Methods and Phenomena* vol 6 (Amsterdam: Elsevier) p 184
[35] Van Roosmalen J A M and Cordfunke E H P 1991 *J. Solid State Chem.* **93** 212